

Using LES to predict ignition sequences and ignition probability of turbulent two-phase flames

A. Eyssartier, B. Cuenot, L.Y.M. Gicquel and T.Poinsot

CERFACS, 42 Av. G. Coriolis 31057 Toulouse cedex 01, France

Abstract

Ignition and altitude reignition are critical issues for aeronautical combustion chambers. The success of ignition depends on multiple factors, from the characteristics of the ignitor to the spray droplet size or the level of turbulence at the ignition site. The optimal location of the ignitor or the potential of ignition success of a given energy source at a given location are therefore parameters of primary importance in the design of combustion chambers. To study ignition, series of experiments are usually performed but they are costly especially when multiple spark locations must be tested. For the same reason, unsteady simulations are useful but do not give an optimal result, unless all locations are tested, which brings the CPU cost to unreasonable values. Alternatives are hence needed and are the objective of this contribution. It is proposed here to derive a local ignition criterion, giving the probability of ignition from the knowledge of the unsteady non-reacting two-phase (air and fuel) flow. This model is based on criteria for the phases of a successful ignition process, from the first kernel formation to the flame propagation towards the injector. Comparison with experimental data on an aeronautical chamber shows good agreement, indicating that the proposed ignition criterion, coupled to a Large Eddy Simulation of the stationary evaporating two-phase non-reacting flow, can be used to optimize the ignitor location and power.

Keywords: Ignition, two-phase flow, turbulent combustion, LES

1. Introduction

Ignition and high altitude re-ignition, are critical processes in aeronautical engines. Efficient and reliable ignition is a crucial point for the certification of

engines, and innovative systems such as laser ignition are actively developed. Ignition is a complex transient phenomenon, not yet fully understood and controlled. Experiments show that ignition by a single spark may be successful or fail in the same operating conditions so that an ignition probability must be used for engine design [1, 2, 3, 4]. This probability is the result of the fluctuations of the fluid state at the igniter location, and is conditioned by local turbulent mixing and velocity fields [5].

Previous numerical studies have been devoted to ignition in premixed gaseous flows [6, 7] and in particular demonstrate the concept of minimum energy for successful ignition [8, 25, 26]. More recently, Quintilla [9] and later Ouarti [10] and Garcia-Rosa [11] used zero and one-dimensional sub-models to describe the very first moments of ignition. Less work has been devoted to the ignition of a two-phase mixture. Ballal and Lefebvre [12, 13] proposed an extension of their analytical study of gaseous ignition to two-phase flow, leading also to the determination of a minimum energy. A comparison with experimental data confirms that global tendencies are captured by their analysis and that ignition is strongly influenced by the droplet size. This study is however limited to a simple and ideal case and misses other processes occurring in a real engine. The complexity of ignition in a real combustion chamber was illustrated by Boileau et al. [14] who simulated the ignition of a full annular combustor. They showed that the ignition process develops in several steps, from the first flame kernel near the igniter, to the stabilisation of a flame on the injector and its propagation towards the neighbouring burning sectors. Such simulations were performed using the Large Eddy Simulation (LES) technique, which has proven its efficiency to compute combustion chambers [15, 16, 17, 18, 19]. LES of non reacting flows is even faster and now used in industry.

There are two ways to use LES to study ignition in turbulent flows:

- perform LES of ignition sequences [20]. This is a very expensive procedure to determine ignition probabilities [3], because a full computation of ignition sequences must be repeated for each spark position.
- build a model based only on a cold flow LES. This requires additional assumptions but is also much faster because it needs only one LES of the flow with the spray but without combustion.

Building a model based on cold flow data is the objective of the present paper. To do this however, we will also use LES results of full ignition sequences to illustrate the statistical nature of ignition and to identify the phenomena which must be included in the model.

For this model called I-CRIT-LES, a general ignition scenario is built, leading to a series of analytical criteria, which are all necessary for successful ignition. These criteria are exclusively based on the non-reacting flow (i.e. before ignition) local conditions, and may be applied to instantaneous realizations of the flow. They allow to understand the controlling processes in ignition and to identify the limiting phenomena in any situation. Then, applying these criteria to a set of instantaneous solutions, used as a statistical sample of the flow, a probability of ignition may be calculated at each point in the combustion chamber.

The paper is organised as follows : first (section 2), LES of full ignition sequences in a swirled kerosene/air flow are presented to illustrate the phenomena which the I-CRIT-LES model will have to take into account. Taking one flow realisation, section 3 establishes the ignition scenarii and criteria. Then section 4 shows how a set of instantaneous flow solutions can be used together with the criteria of section 3 to compute an ignition probability. Finally the model for ignition prediction is applied to a real combustion chamber and compared to experimental results (section 5).

2. LES of ignition sequences

LES of ignition sequences have been performed on the MERCATO configuration from ONERA [4], for which series of experimental ignition tests were available. Several positions of the ignitor were tested at two axial distances (along $z=26\text{mm}$ and $z=56\text{mm}$). The combustion chamber is a simple rectangular box with optical accesses (Fig. 1). For the LES, the position at $z=56\text{mm}$ and $y=57\text{mm}$ was chosen. The fuel injector is typical of aeronautical systems and is made of one swirler and a centered liquid atomiser forming a hollow cone spray. The present case corresponds to kerosene combustion at a mean equivalence ratio of 0.95 (liquid+gas). Air and fuel are both injected at 285K and the mean pressure in the chamber is 1 atm. Mass flow rates of air and kerosene are respectively 35.5g/s and 2.26g/s . LES of the non-reacting two-phase flow were previously performed and validated against measurements [21]. These simulations use the sub-grid scale model WALE [22] associated with no-slip walls. Characteristic boundary conditions NSCBC [23] are used for inlet and outlet sections. A monodisperse Eulerian model as well as monodisperse and polydisperse Lagrangian models have been applied to the dispersed phase and gave similar results for the mean flow [24]. Fig. 2 displays the field of axial mean velocity where the central and

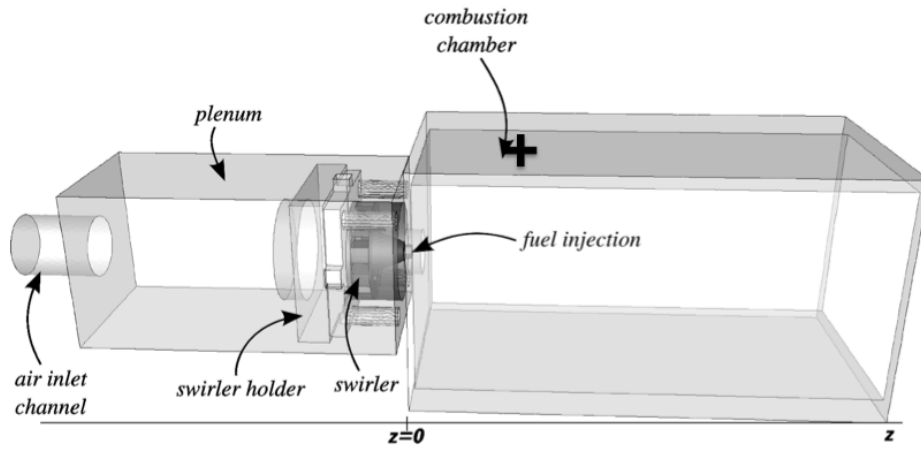


Figure 1: Geometry of the MERCATO burner. Black cross: spark location for ignition sequences (section 2).

corner recirculation zones have been evidenced. All clip planes presented in this section are vertical median planes ($x = 0$). This flow structure controls the droplet distribution, as shown on Fig. 3.

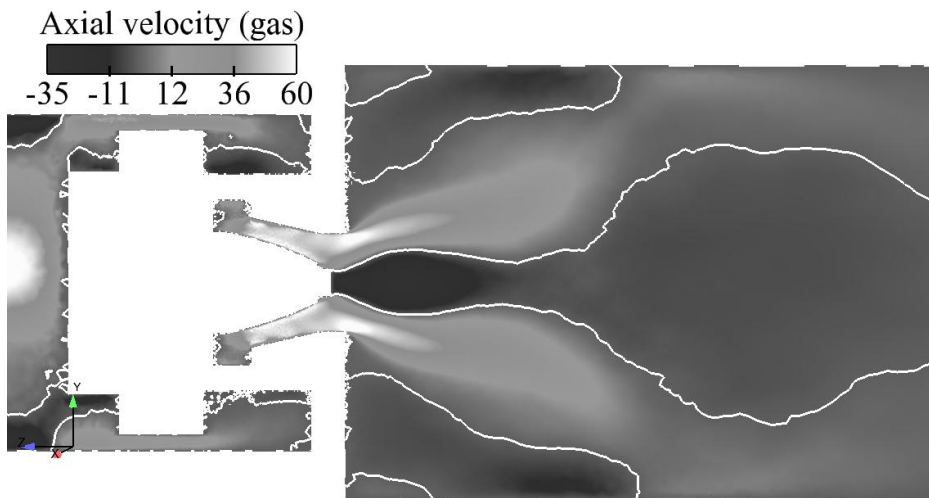


Figure 2: Mean axial velocity field in the $x = 0$ plane (white line denotes 0 m/s)

The hollow cone spray injects locally monodisperse droplets (mean diameter $60 \mu m$) in the high shear zone around the central recirculation zone.

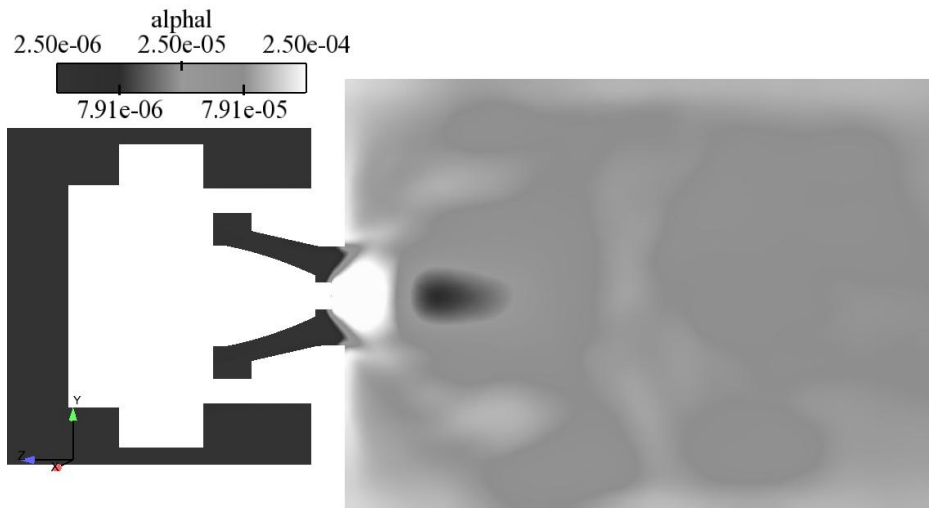


Figure 3: Mean liquid volume fraction field in the $x = 0$ plane

Droplets go around the recirculation zone and partially evaporate before leaving the chamber through the exit.

Starting from this two-phase flow, a series of ignition sequences LES have been performed with the energy deposition model [20] during the sparking phase, the thickened flame model and a two-step reduced chemical scheme during the flame propagation phase for kerosene/air combustion [14]. The energy deposited by the spark has an integrated value of $100mJ$ and lasts $50\mu s$. Eleven ignition sequences were simulated by triggering the spark at 11 different times (i.e. initial flow conditions at sparking time) but always at the same location, producing the 11 curves of Fig. 4. The results of the 11 tests are very different, from fast ignition to immediate failure, also showing a series of intermediate behaviors where ignition starts more or less slowly and leads to complete ignition or failure. The snapshots corresponding to 3 different ignition times t_0 are shown on Fig. 5 after $1ms$ of development. According to Fig. 4, the sizes of the hot gas kernel at this instant are very different. One has already begun to shrink (Fig. 5 a)) and another one has spread rapidly (Fig. 5 c)), while Fig. 5 b) displays an intermediate behaviour, highly wrinkled by turbulence.

Fig. 4 illustrates some of the basic ingredients used in the I-CRIT-LES

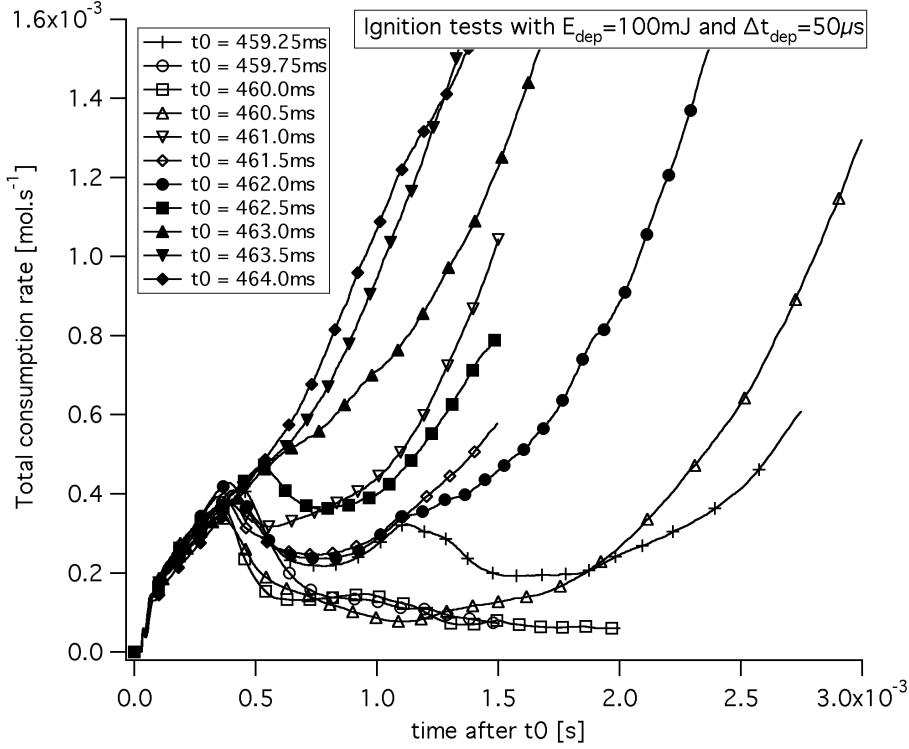


Figure 4: Ignition tests: time evolution of the total consumption rate ($\int \dot{\omega} dV$) in the whole combustor. t_0 being the sparking time.

model: (1) ignition in this turbulent flow is strongly dependent on the instantaneous flow when spark is activated and (2) a model for ignition can not be built on average flow fields: ignition criteria must be applied on multiple realisations of the same flow and ignition probabilities obtained by averaging criteria obtained for these realisations. This is the basis of the I-CRIT-LES model.

3. The ignition criteria

The first step of the I-CRIT-LES model is to build a deterministic ignition criterion on a single non reacting flow realisation obtained by LES. In this work targeted toward aeronautical applications, ignition is produced by a spark or a laser which deposits a certain amount of energy in a cold mixture of gas and droplets. The following ignition sequence is considered as complete and successful if a stabilised flame is installed at the end of the

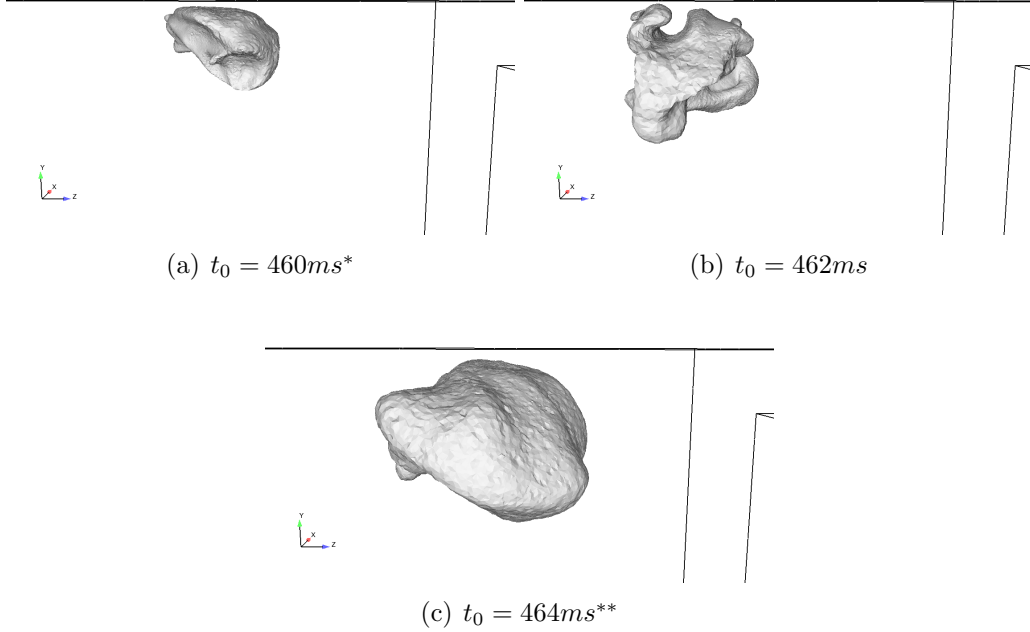


Figure 5: Snapshots of 3 characteristic ignition sequences 1ms after the beginning of the deposition t_0 . The light gray isosurface denotes the $T_{gas} = 1500K$ surface. *: failed ignition ; **: sharp ignition.

process. This criterion does not correspond to the local ignition of the first flame kernel (like in minimum ignition energy studies in premixed flames [25, 26]) but to a global stabilisation test depending on the configuration. The process starts with the creation of a small kernel just after the spark or laser discharge. The deposited energy must be sufficient to sustain this first kernel until combustion takes over and produces sufficient heat to increase the initially sparked hot volume. After reaching a sufficient size, the kernel (which may have been convected to another location in the meantime) starts to interact with turbulence and converts into a turbulent flame. Ignition is completed after this turbulent flame has propagated upwards to the fuel injection system and stabilizes there. In annular combustion chambers (typical of gas turbines), the last phase is the propagation of combustion from one burner to the other. This is a large scale phenomenon which depends on the burner geometry and operating conditions and is not analysed here. It can

be studied with full annular simulations as in Boileau et al. [14].
 The full ignition of one sector can be recast into the following steps (Fig. 6):

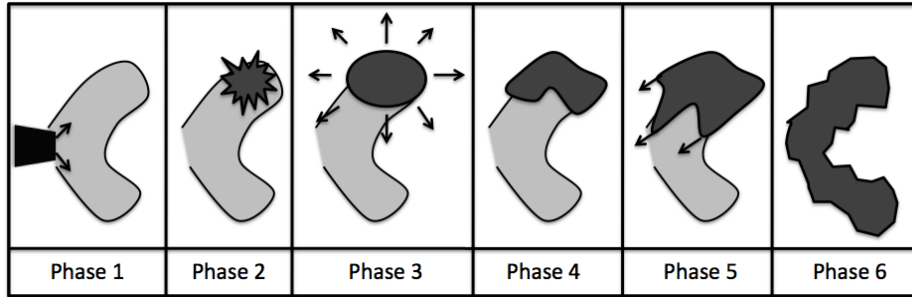


Figure 6: The 6 phases ignition scenario. Dark zones correspond to ignited regions.

1. Droplet dispersion in the chamber (phase 1 in Fig. 6): the first step prior to igniting a burner is to inject fuel and mix it with air. This is described by the LES of a cold (possibly evaporating) two-phase flow, which produces instantaneous distributions of liquid and gaseous fuel in the chamber. The local mixture fraction and velocity fields at the moment of ignition are crucial and are the inputs of the I-CRIT-LES model to determine if the local mixture is flammable or not.
2. Spark or laser discharge and first hot gas kernel (phase 2 in Fig. 6): ignition is triggered by an energy deposition which leads to complex processes including non-equilibrium physics. If sufficient, the energy deposition leads to the creation of a small hot gas kernel. The size and temperature of this first kernel are critical for its later growth.
3. Growth and convection of the kernel (phase 3 in Fig. 6): if conditions are favorable, combustion starts around the hot gas. If the vaporisation time is small compared to the heat diffusion time, the hot gas kernel becomes a flame kernel and its size increases [13].
4. Transition to a turbulent flame (phase 4 in Fig. 6): after reaching a size comparable to the smallest turbulent structures, the flame kernel starts

to interact with turbulence, leading to wrinkling and stretching of the flame front. In most situations, this will accelerate flame propagation. If turbulence is too strong however, flame quenching may occur [27]. This last point is not considered in the present analysis as turbulent quenching is not expected to be a major mechanism in the target applications. However another quenching mechanism may occur in case of flame interaction with cold walls and is considered in the present analysis during Phase 4.

5. Propagation of the turbulent flame towards the injection system (phase 5 in Fig. 6): usually the ignition system is located downstream of the injection system, and the turbulent flame kernel is created away from the stationary flame position of the ignited burner. In order to stabilize near the injector, the turbulent flame must propagate upstream, i.e. against the mean flow. This is possible only in low velocity zones, around or in recirculation zones, and requires a turbulent flame speed larger than the local flow speed.
6. Stabilisation of the flame: this is the end of the ignition process of a single burner. It is considered as automatically satisfied if all phases 1 to 5 are fulfilled.

For the full annular burner ignition a seventh step should be added, corresponding to flame propagation from ignited burners to their neighbours [14]. This last step is not considered here.

Steps 1 to 5 are associated to five conditions that must be fulfilled for the successful completion of each step and the start of the next one :

C1 (step 1): The fuel distribution must guarantee a flammable mixture.

C2 (step 2): The discharge energy must be sufficient to create a first hot gas kernel.

C3 (step 3): The local conditions (vaporisation time versus diffusion time) must allow the kernel to increase.

C4 (step 4): The flame must not be quenched near walls.

C5 (step 5): The flame speed must be larger than the local flow speed to allow the flame to propagate upwards.

These conditions will now be expressed in terms of criteria which depend on the instantaneous flowfields and change from one flow realisation to another.

Criterion 1: Flammability

During a two-phase flow ignition, the available fuel is the fuel vapor (usually small) and the liquid fuel which will evaporate at the spark location. As a consequence, flammability of the mixture is evaluated by the total (gas + liquid) equivalence ratio, that must be in the flammability limits of the considered fuel. Defining the equivalence ratio as:

$$\Phi = \Phi_{gas} + \Phi_{liq} = s \frac{Y_F}{Y_O} + s \frac{\rho_l \alpha_l}{\rho Y_O} \quad (1)$$

where s is the stoichiometric ratio, Y_F and Y_O respectively the fuel and the oxidizer mass fraction, ρ the gas phase density, ρ_l the liquid phase density and α_l the liquid mass fraction. Criterion 1 writes:

$$\Phi_{low} \leq \Phi \leq \Phi_{high} \quad (2)$$

where Φ_{low} and Φ_{high} are respectively the low and high flammability limits, known for usual fuels.

Criterion 2: Energy discharge and first kernel

Spark ignition has been described in details by R.Maly and R.Vogel [28]. They recalled that three phases (or discharge modes) can usually be distinguished. The first one is the breakdown phase. It lasts several nanoseconds (1-10 ns) and is the scene of very high voltage (about 10 kV) and currents (about 200 A). It implies the creation of a cylindrical plasmatic channel between the two electrodes, where temperature and pressure can respectively reach several tens of thousands degrees and 200 bars. The breakdown phase is very efficient as very few energy losses are observed. The following phases are the arc and glow discharges. Voltage, current and number of ionized particles are much lower but this phase is much longer (hundreds of microseconds to milliseconds) and heat losses due to conduction in the electrodes become very important.

Kono et al. [29] and later Kravchik and Sher [7] underlined that first, mass and energy transfers are controlled by the high pressure wave (blast wave) created by the breakdown. While expanding at high velocities, the shape of the kernel changes and quickly becomes spherical [7, 30]. At the same

time, ionization plays a crucial role by releasing energy that slows down the cooling of the kernel [7, 30]. This fast expansion phase ends only after about one hundred microseconds, and is followed by a slower expansion due to heat conduction and mass diffusion. Although the plasma phase corresponds to the highest heat transfer and gas temperature, it is too short and strong to be a limiting process of ignition and is therefore not described here. In fact, the crucial parameter is the fluid state at the end of the plasma phase (when the gas has come back to equilibrium), resulting from the true amount of energy transferred to the gas at the end of the discharge. This amount has been evaluated and measured by several authors [28, 31] and is typically 10 to 30% of the spark energy.

For laser ignition, the energy deposit is simpler to evaluate since lasers directly transfer almost the whole energy to the gas, even if a part of this energy can produce a strong pressure wave through the dilatation of the ionized gas [32].

The previous observations were obtained for pure gaseous mixtures. In a spray, droplets evaporation is much slower than the energy transfer from the igniter to the gas: it is assumed here that droplets do not interact directly with the igniter and are heated only by their interaction with the hot gas (see Fig. 7). Furthermore, in practical devices, the spray is very diluted at the spark location so that the energy absorbed by the liquid is very small.

The minimum energy required to install a first kernel is determined by considering the heating, evaporation and ignition of a homogeneous mist of droplets in an initially fuel-vapor free gaseous environment (Fig. 7).

Numerical tests (see Appendix A) show that if the liquid is too far from saturation conditions when combustion starts, evaporation is too slow to feed the flame so that a criterion can be defined by introducing an ignition temperature T_{ign} which is the temperature at which the chain-branching reaction balances the terminating reaction [34]. This may be expressed in terms of a gas temperature, that must stay above the ignition temperature T_{ign} until the liquid has reached its saturation temperature T_{cc} . If t_{cc} is the time at which the liquid reaches saturation, criterion 2 is:

$$T(t_{cc}) \geq T_{ign} \quad (3)$$

It requires the knowledge of the gas temperature temporal evolution $T(t)$, which is obtained from the evolution equations for the gas (T) and liquid (T_l)

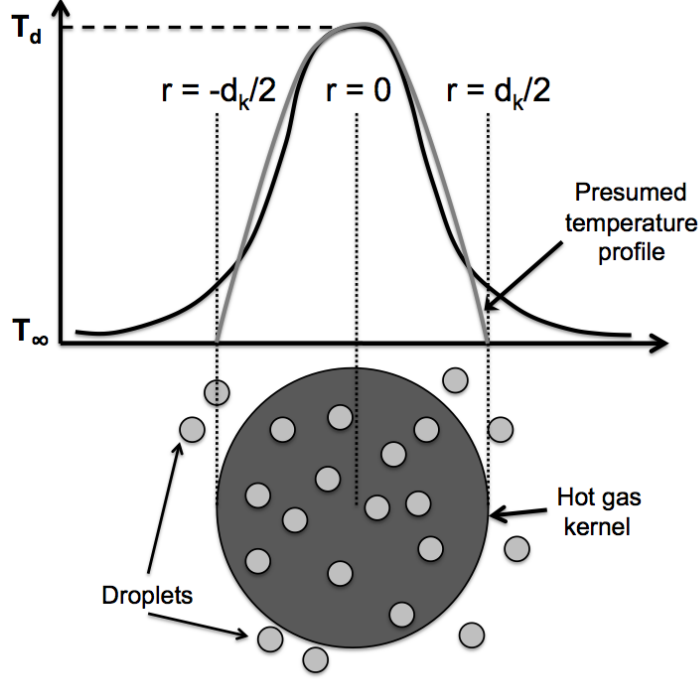


Figure 7: Sketch of the topology considered with the representation of the temperature profile at the end of the energy deposition.

temperatures at the spark location (typical evolutions are shown in Fig. 8), taking into account heat diffusion, heat transfer between the two phases and a source term (the spark energy during the deposition phase, $S = \dot{e}_{dep}$) in a simplified form (see Appendix B for detailed developments):

$$\frac{\partial T}{\partial t} = \frac{T_\infty - T}{\tau_{diff}} + \frac{T_l - T}{\tau_{cond}} + \frac{S}{\rho C_p} \quad (4)$$

$$\frac{\partial T_l}{\partial t} = -A \frac{T_l - T}{\tau_{cond}} \quad (5)$$

These equations are written for the sparking phase and the heating phase of the droplets, before they reach T_{cc} , therefore with negligible evaporated fuel, i.e. negligible combustion. A unity Lewis number is assumed. The initial temperatures for the gaseous and for the liquid phase are respectively noted T_∞ and $T_{l,0}$. $T_d = T_\infty + e_{dep}/\rho C_p$ is the gas temperature at the end of the

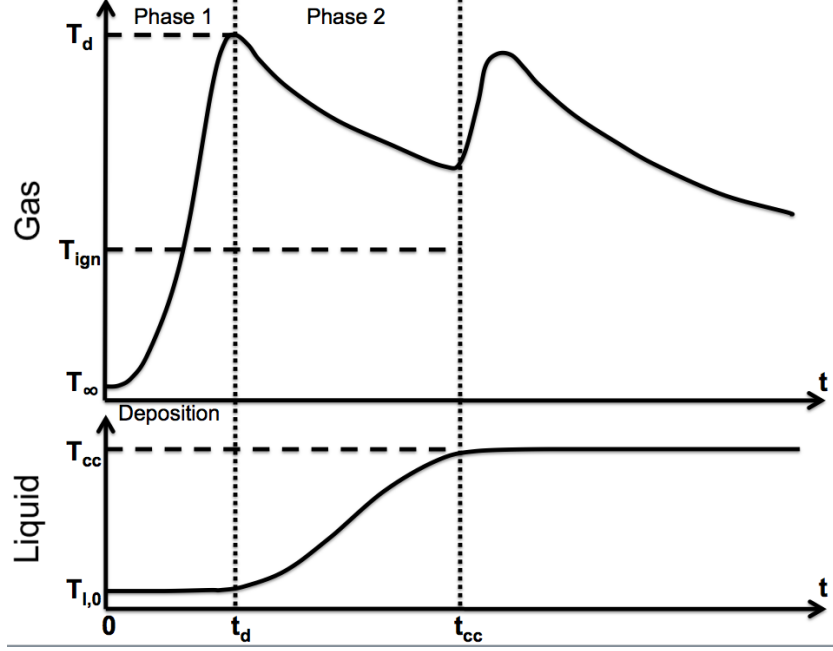


Figure 8: Typical evolutions of the temperatures when ignition occurs (thermal runaway after t_{cc}).

energy deposit phase, e_{dep} being the volumic energy deposit. The parameter $A = \rho C_p / \alpha_l \rho_l C_{p,l}$ is the liquid to gas ratio of heat capacity, with α_l the liquid volume fraction. The two characteristic times $\tau_{diff} = d_k^2 / 8n_{dim}D$ and $\tau_{cond} = d_l^2 / 6D\alpha_l Nu$ describe heat diffusion in the gas and heat transfer between the phases, n_{dim} being the number of dimensions. In these expressions, D is the heat diffusion, d_k is the kernel size, and d_l is the droplet diameter. Solving these two equations yields:

$$T(t_{cc}) = T_d - \frac{\tau_{cond}}{a\tau} (T_{cc} - T_{l,0}) \quad (6)$$

where $1/\tau = 1/\tau_{diff} + 1/\tau_{cond}$. Finally criterion 2 becomes:

$$\frac{e_{dep}}{\rho C_p} \geq (T_{ign} - T_\infty) + \frac{\tau_{cond}}{a\tau} (T_{cc} - T_{l,0}) \quad (7)$$

or

$$\frac{e_{dep}}{\rho C_p} \geq (T_{ign} - T_\infty) + \left(\alpha_l + \frac{4n_{dim}}{3Nu} \frac{d_l^2}{d_k^2} \right) \frac{\rho_l C_{p,l}}{\rho C_p} (T_{cc} - T_{l,0}) \quad (8)$$

This criterion expresses that the energy deposit must be sufficient to heat the gas from T_∞ to at least T_{ign} and the liquid from $T_{l,0}$ to T_{cc} while the gas temperature does not cool down to a temperature lower than T_{ign} . Also notice that $d_l = 0$ (i.e. and $\alpha_l = 0$) provides the gaseous limit of the criterion, i.e. the minimum ignition energy density for a gaseous premixed flow.

Criterion 3: Kernel growth

The next step is to sustain the kernel and corresponds to phase 3 in Fig. 6. If combustion is not strong enough, the heat release is not sufficient to compensate for the cooling of the gas due to diffusion and the kernel quenches.

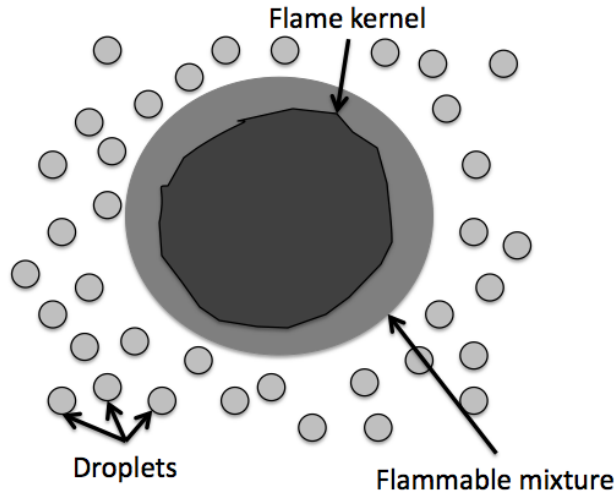


Figure 9: Expansion of the initial laminar kernel.

This third criterion is derived following the methodology of Ballal and Lefebvre (1981)[13]. Considering a hot gas kernel surrounded by a flame, in a mixture of fresh gas and droplets (Fig. 9), characteristic times of evaporation τ_{vap} , diffusion τ_{diff} and combustion τ_{comb} are compared. Combustion is sustained if the droplets can evaporate and burn before heat diffuses away:

$$\tau_{vap} + \tau_{comb} \leq \tau_{diff} \quad (9)$$

As combustion is fast compared to diffusion and evaporation, $\tau_{comb} \approx 0$. The vaporization time is determined from the evaporation mass transfer as expressed in Spalding's theory [35]:

$$\tau_{vap} = \frac{\rho_l d_l^2}{6\Phi Sh \rho D \ln(1 + B_M)} \quad (10)$$

where B_M is the mass Spalding number. After rearrangement of Eq. 9, one finds criterion 3:

$$\frac{d_k}{d_l} \geq \sqrt{\frac{4n_{dim}\rho_l}{3\Phi Sh \rho \ln(1 + B_M)}} \quad (11)$$

which compares the kernel size d_k to the droplet size d_l . If the kernel size is too small compared to the droplet diameter, heat diffusion is too fast compared to evaporation and the flame can not survive.

Criterion 4: Wall quenching

Previous studies [36, 37, 38, 39] have shown that a flame can not exist at a closer distance to the wall than a critical distance called the quenching distance δ_Q . Therefore a flame ignited too close to a wall will not be able to survive. The quenching distance has been evaluated for various laminar flames interacting with walls, and is usually expressed as a Peclet number $Pe_Q = \delta_Q/\delta_l^0$ where δ_l^0 is the local laminar flame thickness. This number is of order of 3.0 for usual hydrocarbons (1.7 for H_2/O_2) when the flame propagates normally to the wall (Head On Quenching). A characteristic time of the interaction t_Q is also defined, which represents the time to quench the flame. This time is also given in a non-dimensional form $\tau_Q = t_Q/t_l^0$ where $t_l^0 = \delta_l^0/S_l^0$. For typical hydrocarbons $\tau_Q \approx 2.1$. We also define δ as the distance of the ignition kernel to the wall.

Knowing Pe_Q and τ_Q , criterion 4 is expressed differently depending on the wall distance δ (Fig. 10):

- First, if the kernel is initiated within the quenching layer, i.e. if $\delta \leq \delta_Q$, it has to leave this zone before $t = t_Q$, then:

$$\delta \leq \delta_Q \quad \& \quad U.n > \frac{\delta_Q - \delta}{t_Q} > 0 \quad (12)$$

where U is the local flow velocity and n the wall normal.

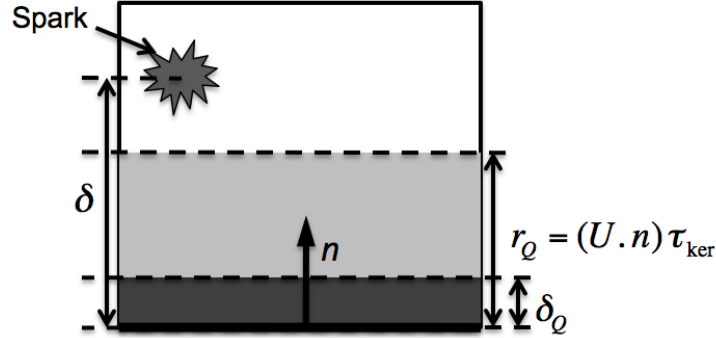


Figure 10: Layers description of criterion 4

- Second, even if $\delta > \delta_Q$, the flame may convect within the quenching layer. Hence, it has to be strong enough before entering this zone. It is assumed that the flame is strong enough when it has developed during at least $\tau_{ker} = t_{cc} + \tau_{diff}$ which represents the time to reach equilibrium (i.e. non super adiabatic temperature). This leads to the definition of an "overlayer distance" $r_Q = (U \cdot n) \tau_{ker}$ and the second case as:

$$r_Q \geq \delta > \delta_Q \quad \& \quad U \cdot n > 0 \quad (13)$$

- At last, if:

$$\delta > r_Q \quad (14)$$

criterion 4 is validated independently of other conditions.

Criterion 5: Upstream flame propagation

The turbulent flame created in step 5 must propagate upstream and ignite the complete chamber. This is a complex issue requiring full LES of ignition sequences (something we do not want to perform to use the present model) or Lagrangian simulations of the kernel trajectory (see for ex [40]). To construct a criterion based only on instantaneous snapshots, criterion 5 in I-CRIT-LES considers a simpler condition, stating that the flame velocity must allow the

front to propagate upstream: the turbulent flame speed S_T must be larger than the flow velocity U :

$$U - S_T \leq 0 \quad (15)$$

where U is the flow mean velocity and $S_T \approx S_L^*(\Phi) + u'$ is the turbulent flame speed [41, 42] with u' being the turbulent velocity fluctuation. The laminar flame speed $S_L^*(\phi)$ for two-phase flow flames is corrected for lean combustion as in [13]:

$$S_L^*(\phi) = \left(\frac{\tau_{vap}}{D} + \frac{1}{(S_L^0)^2} \right)^{-1/2} \quad (16)$$

Global ignition index

All five criteria are necessary for ignition and are combined in an ignition index $I_{ign} = C_1 \times C_2 \times C_3 \times C_4 \times C_5$, where C_i takes the value 1 if criterion i is verified and 0 otherwise. At this stage, the ignition index is applied to one flow snapshot and is a deterministic quantity which can take only 0 or 1 values. Typical evolutions of the index I_{ign} are shown in Fig. 11 and Fig. 12. Criterion 1 for example (flammability, Fig. 11a) does not depend on droplet diameter or on spark energy. Criterion 2 (first kernel creation) depends on the droplet diameter and spark energy but the liquid volume fraction has almost no influence. On the other hand, the growth of the kernel (Criterion 3 Fig. 11c) is controlled by the droplet diameter. Finally, the global index can take complex dependances (Fig. 11d) when it is plotted versus droplet diameter, spark energy and fuel liquid mass fraction.

Sensitivity to pressure, initial gas temperature and droplet diameter

The first three criteria, C_1 to C_3 are local and it is interesting to study their sensitivity to P , T_∞ and d_l space. Here the energy deposit $E_{dep} = 50mJ$ and the liquid volume fraction $\alpha_l = 3.10^{-4}$ are fixed. To first order, Fig. 12 shows that ignition is more difficult at high pressure: almost all criteria become 0 when pressure is higher than 30 bars. The maximum pressure at which ignition becomes impossible will be called P_{il} and isosurfaces of P_{il} versus gas temperature and initial droplet diameter correspond to the transition of light to dark zones in Fig. 12. For criterion 1 (flammability limits), P_{il} varies mainly with temperature: higher initial temperatures lead to eas-

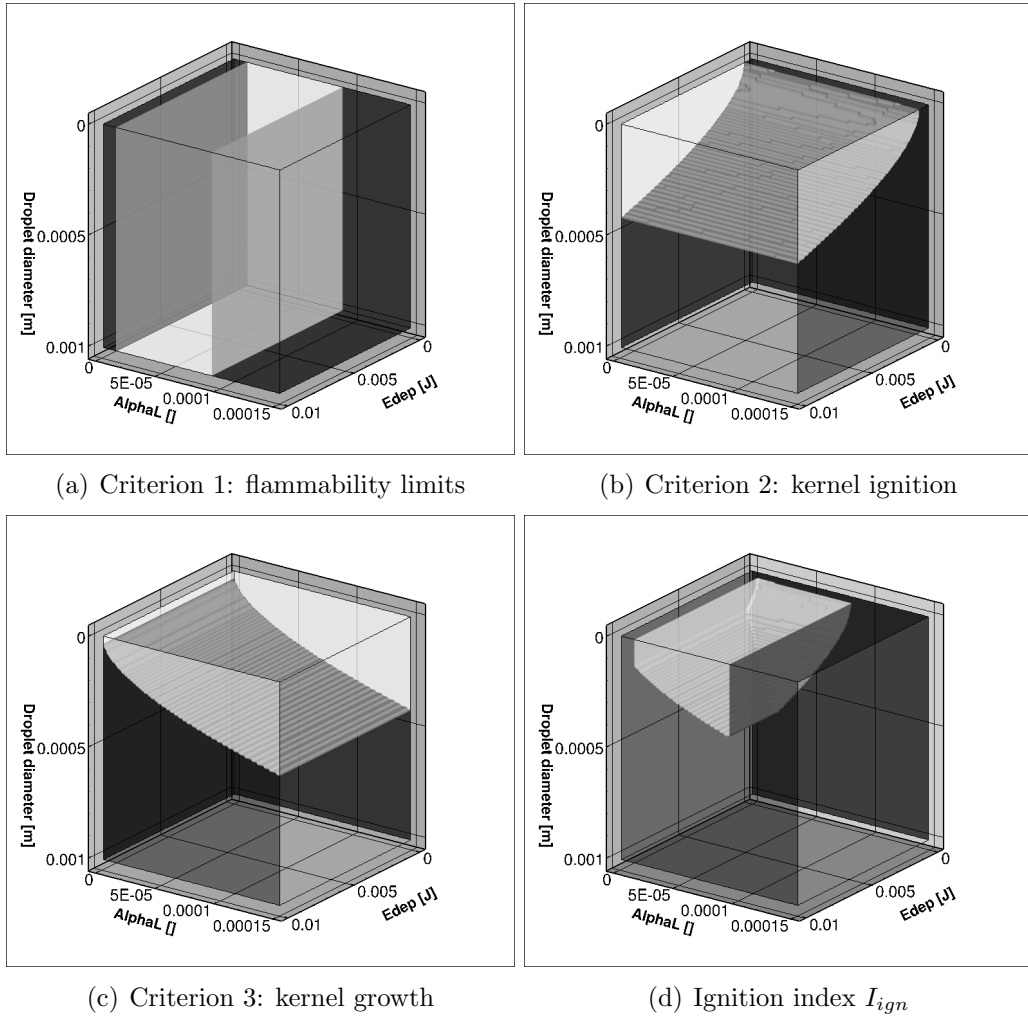


Figure 11: Isosurfaces of limits of validity of ignition criteria and the full index function of the liquid volume fraction, the droplet diameter and the energy deposit (light part means the criterion is validated, i.e. = 1).

ier ignition and higher values of P_{il} . The second criterion (kernel ignition) is even more sensitive to temperature (Fig. 12b) but the third one (kernel propagation in Fig. 12c) leads to a limit pressure P_{il} depending mainly on the droplet diameter. Finally, the resulting surface for P_{il} obtained from the combinaison of criterion 1 to 3 leads to the complex shape of Fig. 12d.

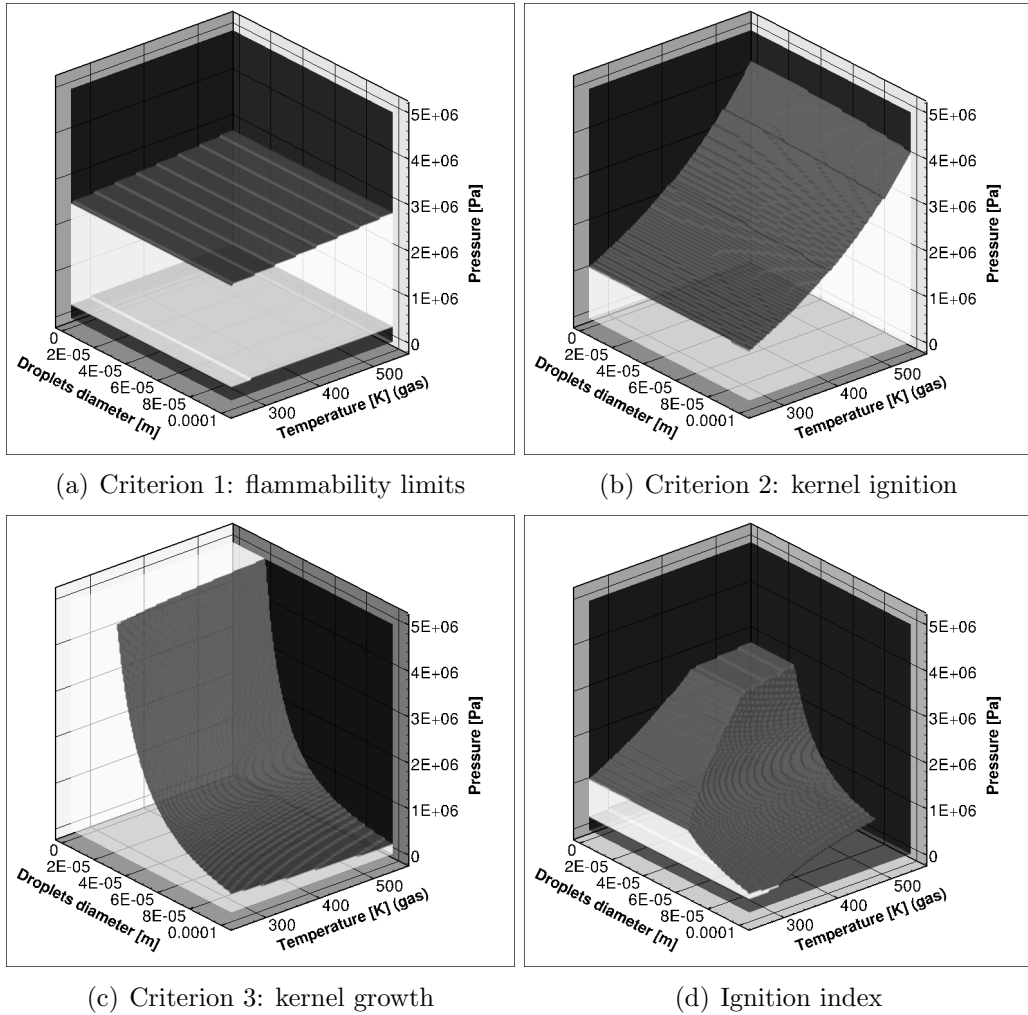


Figure 12: Isosurfaces of limits of validity of ignition criteria and the global index as functions of the pressure, the initial gas temperature and the droplets size (light part means the criterion is validated, i.e. = 1). The spark energy is 50 mJ and the initial fuel volume fraction is $\alpha_l = 3.10^{-4}$

4. Ignition probability

The ignition scenario and criteria described in section 3 are developed in a fully deterministic framework: given initial conditions, the model predicts if ignition will be successful or fail with a 0 or 1 ignition index. However ex-

act conditions (temperature and composition of the liquid and gas phase) at the location and moment of ignition fluctuate due to turbulence and control the success of the ignition sequence.

Fig. 4 was obtained through expensive LES and justifies the development of the present model: it would be much too expensive to perform series of ignition sequences with LES at each igniter location to obtain ignition probabilities. A probabilistic model is a better choice and the I-CRIT-LES uses non-reacting LES (which is unique and much faster) to evaluate ignition probability without actually simulating ignition events. In this approach, each instantaneous LES solution is viewed as one flow realisation, the finite set of instantaneous fields being used as a statistical ensemble of samples representative of the turbulent field. This requires that the solutions are taken after statistical convergence has been reached. Applying criteria C_1 to C_5 to a series of N realisations (instantaneous solutions at $t = t_k$) allows to build a probability for the local ignition index:

$$p(I_{ign}) = \frac{1}{N} \sum_{k=1}^N I_{ign}(t_k) \quad (17)$$

This statistical estimate is a three-dimensional field giving the probability of completion of all ignition steps at each location in the burner, and varies from 0 to 1 (by construction). Using the same definition, one can also build an individual probability which is specific to one criterion replacing $I_{ign}(t_k)$ by $C_i(t_k)$, and showing how a step of the ignition will behave. If we suppose statistical independence of the criteria C_1 to C_5 one can write $p(I_{ign}) = \prod_{i=1}^5 p(C_i)$, where the probabilities $p(C_i)$ are built as in equation 17. Tests (not presented here) showed that these two definitions of $p(I_{ign})$ do not provide the same results. Hence, the criteria C_1 to C_5 are not statistically independent, especially C_2 and C_3 (the amount of the energy deposit will directly influence the size of the kernel at the beginning of the phase 3, Fig. A.16).

The present approach also allows to analyse the causes of failure when the ignition probability, $p(I_{ign})$, is lower than 0.5, identifying the limiting criterion as the criterion with the lowest probability $p(C_i)$. The same analysis may be conducted on only one instantaneous solution, identifying the cause of failure by the first criterion for which $C_i = 0$. In this case the analysis is deterministic.

5. Application to an aeronautical chamber

The I-CRIT-LES model was applied to the MERCATO configuration described in section 2. The first test was to check if I-CRIT-LES was able to match the success/failure of individual deterministic ignition sequences presented in section 2. For each test, only one LES solution is used (the one at the corresponding t_0), hence the value is binary (0 or 1). The results are shown on Fig. 13. The methodology predicts no ignition for $t_0 = 459.75ms$ and $460ms$, almost no ignition for $t_0 = 459.25ms$ and $460.5ms$ but with favorable zones for ignition very close to the spark, and ignition for the others (especially for $t_0 = 464ms$). These observations are in very good agreement with the previous ignition sequences performed. Like in Fig. 4, failure of ignition at time 459.75ms and 460ms are predicted as well as the sharp ignition at time 464ms. I-CRIT-LES does not predict late ignition phenomena ($t_0 = 459.25ms$ and $460.5ms$), as this involves convection of the kernel (i.e. trajectory computations) which are very expensive and can not be captured simply by analytical models.

The main purpose of this index is to provide statistics about ignition. In the experiments [4], several positions of the ignitor were tested (along $z=26mm$ and $z=56mm$) and for each one, the ignition probability was calculated from the recording of success/failure of ignition. A direct comparison with the present model is thus possible.

To obtain ignition probabilities, the ignition index is built taking 200 independent instantaneous LES solutions over a total time of 20ms. The result is shown in Fig. 14, showing that ignition is most probable in recirculation zones and is almost impossible close to the fuel injection and at the bottom chamber ($z = 0$ plane in Fig. 1) as well as high speed zones. The probability is intermediate in the region surrounding the recirculation zones. This result is in good agreement with experimental findings, indicated with the black and white arrows in the figure, except around the fuel injection axis where the predicted probability is high (i.e. white) while no ignition could be obtained experimentally. This is however explained by the fact that the laser ignitor used in the experiment could not be focused at the center of the domain due to the presence of the spray and its diffraction effect on the laser beam.

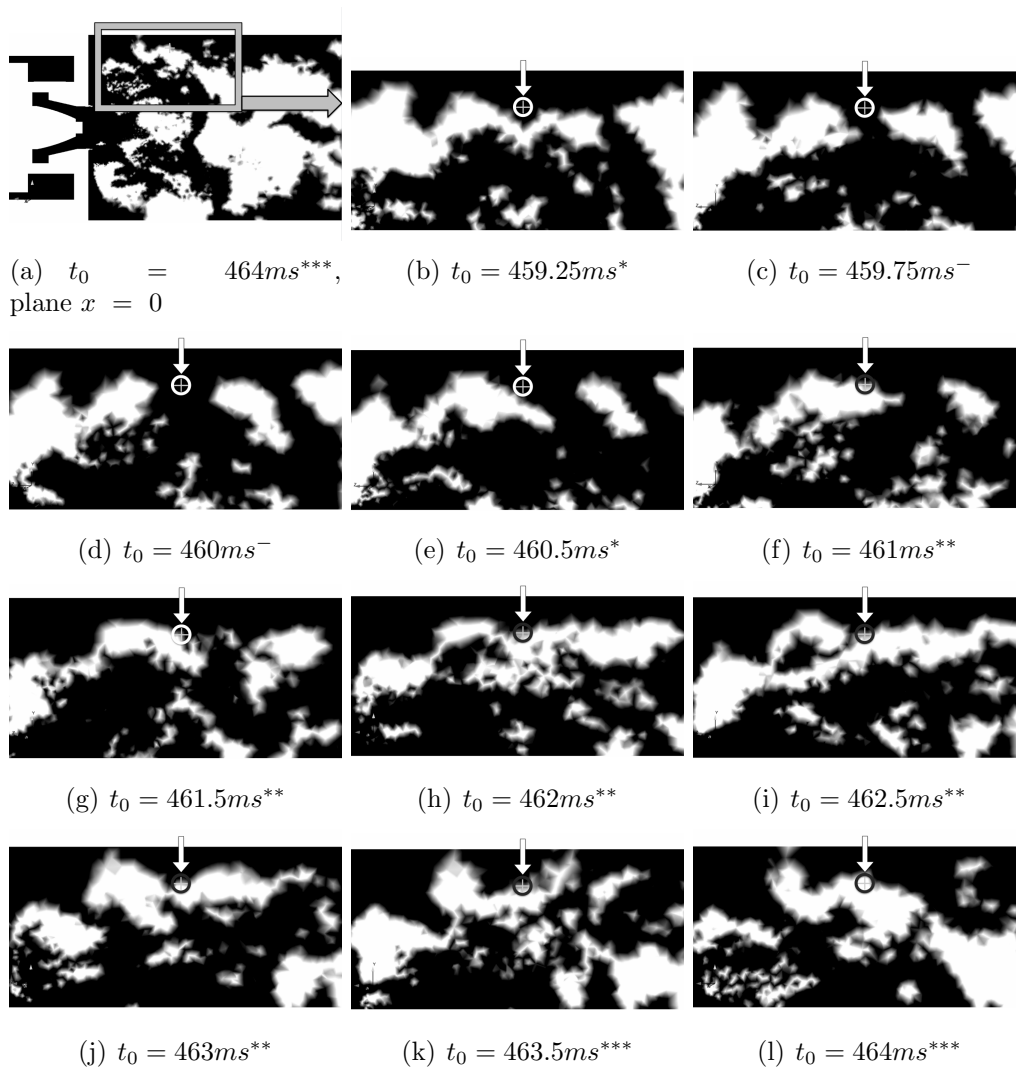


Figure 13: I-CRIT-LES applied to single snapshots for the same times as in section 2. White: I-CRIT-LES=1 (ignition) ; Black: I-CRIT-LES=0 (no ignition). Reminder of Fig. 4: circle denotes spark location. $-$: failed ignition ; $*$:late ignition ; $**$: successful ignition ; $***$: sharp ignition.

In order to better understand the cause of ignition failure, the local limiting criterion is displayed in Fig. 15. The values 1 to 5 correspond to the criterion with the lowest probability (over all realisations). The value 6 indicates that all criteria are validated and ignition is highly probable (more than 0.5).

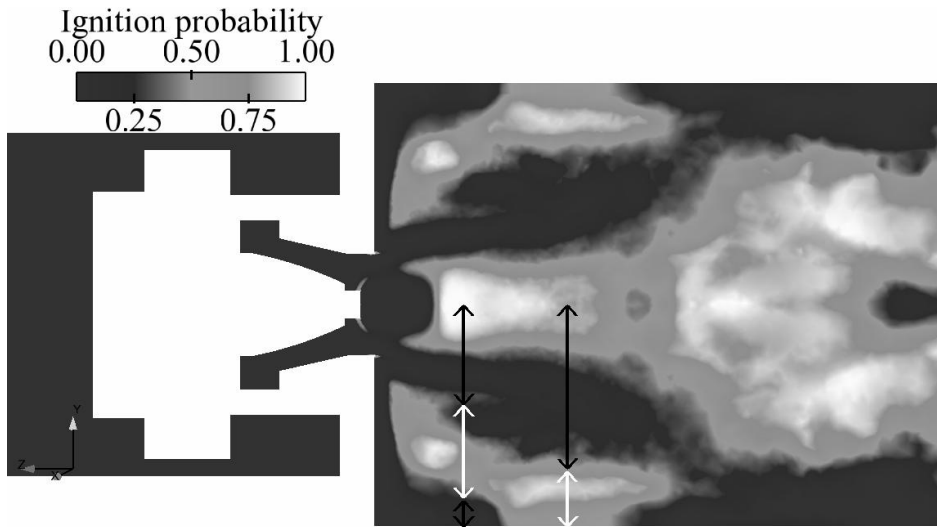


Figure 14: Global ignition index in the $x = 0$ plane given by I-CRIT-LES for $E_{dep} = 100mJ$. Dark zones correspond to low ignition probability. Arrows report experimental tests (white means ignitions have been observed, black means no ignition observed)

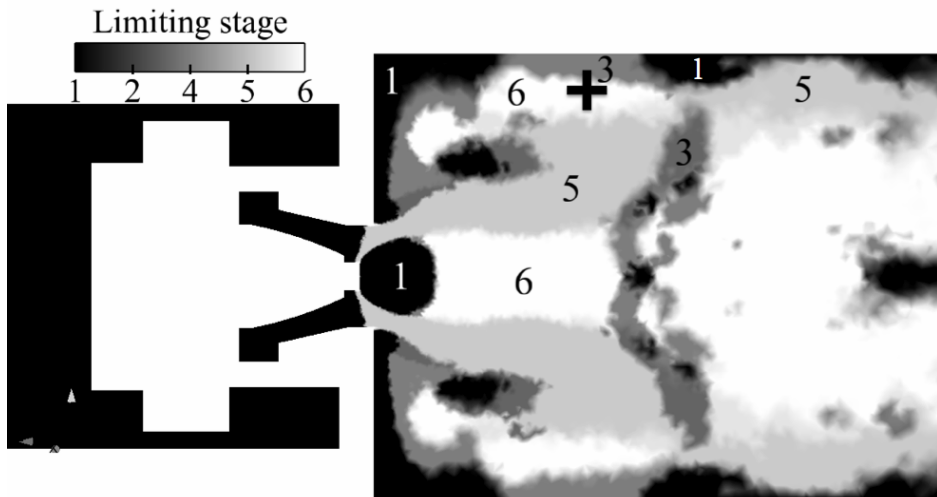


Figure 15: Limiting criterion in the $x = 0$ plane. Black cross: spark location for ignition sequences simulations. $E_{dep} = 100mJ$

Figure 15 provides an identification of the mechanism leading to failed

ignition: dark regions correspond to a failure of criterion 1, i.e. flammability limits. The first dark zone is at the fuel injector nozzle, where droplets accumulate because of the recirculation zone just downstream yielding a mixture that is too rich. The second dark zone corresponds roughly to a low speed area of the lateral recirculation zone, where the droplets also accumulate. The last dark region (next to the top and bottom walls) corresponds to the impact of the main flow on the wall. Criterion 2 is always fulfilled, meaning that the energy deposit is always sufficient in this case. In gray, criterion 3 indicates that evaporation is too slow compared to diffusion to sustain the flame kernel. Criterion 4 applies only in a thin zone near the wall. Finally criterion 5 in light gray is limiting in zones of strong axial velocity, in the shear zone around the central recirculation: the turbulent flame speed is not sufficient to propagate the flame in the upstream direction.

An alternative use of the ignition index is to determine the minimum ignition energy (MIE) to be provided for successful ignition: this point is reached when criterion 2 becomes the most restrictive. Since the kernel diameter d_k depends on the energy deposit, criterion 3 is also affected and can decrease dramatically in some regions. For this operating point, it was found that a minimal energy of about 20mJ was necessary to have relatively large area (about few d_k large) of non zero probability to ignite the chamber (the experimental tests were done with an energy from 60 to 212mJ, its purpose was not to evaluate the MIE) .

6. Conclusions

Ignition sequences using LES have been performed in 1D and in 3D in the MERCATO configuration. These simulations underlined the large variability of the ignition process and its different phases. An analytical model, I-CRIT-LES, to predict ignition probability of liquid-gas mixtures from non-reacting fields in any configuration has been presented, based on the identification of the successful ignition and propagation mechanisms and the derivation of associated criteria. The probabilistic aspect is recovered by applying the ignition criteria to a series of independent LES snapshots. Application to a real combustor allows to identify the best ignitor locations and the causes of failure in the other regions. A comparison with experimental tests shows that the model captures the zones of high and low ignition probabilities and can be used to compute the correct optimal locations for ignition.

Appendix A. Validation of criterion 2 using 1D Direct Numerical Simulation (DNS)

To take into account the size of the energy deposit, one-dimensional simulations were performed to study the evolution of the two-phase mixture (Fig. A.16) and to test the criterion associated (Fig. A.18). This is a simple 1D DNS where a two-phase mixture of air and kerosene (only liquid initially and monodisperse droplets) is ignited by a 1D spark for which the local energy deposited by unit volume is [20]:

$$\dot{e}_{dep}(x, t) = \frac{E_{dep}}{(\sqrt{2\pi})^2 \sigma_x \sigma_t} e^{-\frac{1}{2} \left(\frac{x-x_0}{\sigma_x}\right)^2} e^{-\frac{1}{2} \left(\frac{t-t_0}{\sigma_t}\right)^2} \quad (\text{A.1})$$

where $E_{dep} = \int \dot{e}_{dep} dt dV = \int e_{dep} dV$ is the total amount of energy transferred by the spark to the gas, σ_x and σ_t are parameters that control the size and duration of the source term, x_0 and t_0 are the space and time coordinates of the deposit. Initial conditions are $P = 1atm$ with a temperature of $300K$ for both phases. The droplets size is $60\mu m$ and the liquid mass fraction 10^{-4} . The spark characteristics are: $\sigma_x = 0.5mm$ and $\sigma_t = 8.2\mu s$. The liquid fuel is kerosene (surrogate and chemical kinetic scheme from Franzelli and Riber (2010) [33]).

The temporal evolution of the droplet (dashed line) and gas (solid line) temperatures are shown in Fig. A.16. In a first phase ($t \leq t_d$), the gas temperature increases sharply, under the effect of the energy deposition. Then in a second phase ($t_d \leq t \leq t_{cc}$), heating of the droplets starts, while the gas cools down. After some time, the droplets reach their equilibrium temperature T_{cc} , while the combustion reactions, activated by the hot gas temperature, start to release heat, resulting in a fast increase of the gas temperature and a second temperature peak at $0.4ms$. This last step corresponds to the creation of a first kernel.

If during the spark does not rise the gas temperature enough, the gas may be cooled too strongly by heat diffusion, and the fuel evaporation is too small, reactions can not start and ignition fails (dashed-dotted lines in Fig. A.17).

A series of ignition simulations were performed for the parametric study of the droplet size d_l and of the energy of the spark E_{dep} , keeping all other parameters unchanged. The resulting ignition map is compared to criterion 2 in Fig. A.18, showing that criterion 2 correctly predicts ignition limits for the presented test cases.

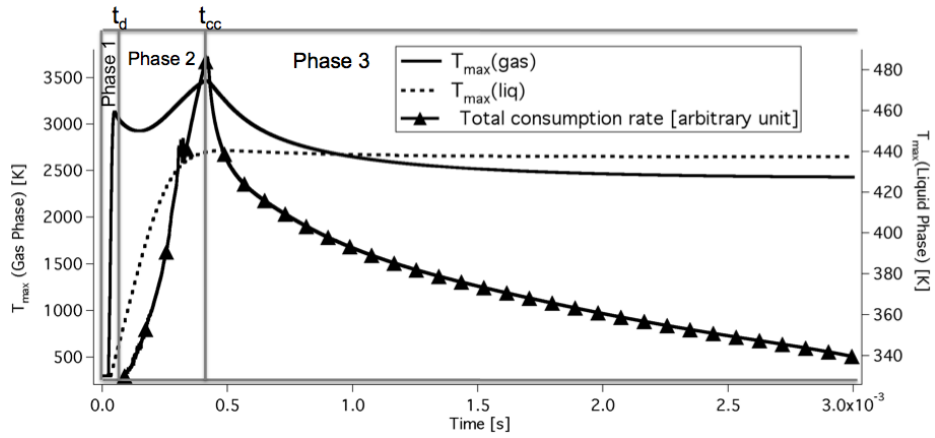


Figure A.16: Ignition of a homogeneous droplet cloud ($E_{dep} = 4.3mJ$).

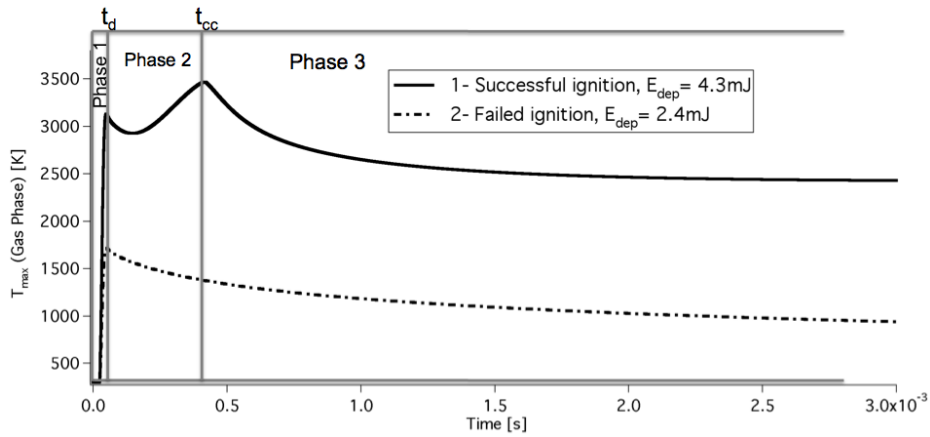


Figure A.17: Comparison of the temporal evolution of maximum gas temperature between successful (1) and failed (2) ignition.

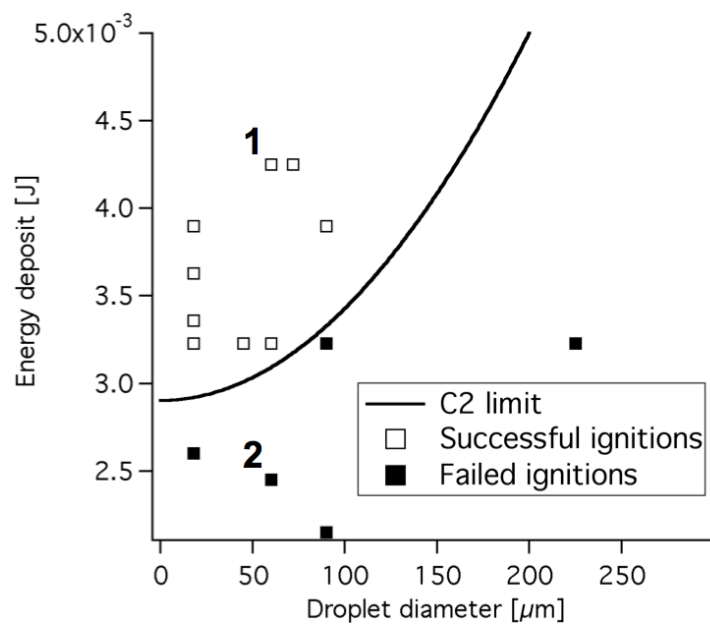


Figure A.18: Minimal energy as a function of droplet diameter d_l for a stoichiometric mixture. 1 and 2 refer to Fig. A.17.

Appendix B. Criterion 2 developments

The evolution equations for the gas (T) and liquid (T_l) temperatures at the spark location, taking into account heat diffusion, heat transfer between the two phases and a source term S (the spark energy during the deposition phase, see phase 1 in Fig. 8 and Fig. A.16) are:

$$\frac{\partial T}{\partial t} = \frac{\lambda}{\rho C_p} \Delta T + \frac{\Phi}{\rho C_p} + \frac{S}{\rho C_p} \quad (\text{B.1})$$

$$\frac{\partial T_l}{\partial t} = -\frac{\Phi}{\alpha_l \rho_l C_{pl}} \quad (\text{B.2})$$

where λ is the thermal conductivity, ρ the gas density, ρ_l the liquid density and C_p the thermal capacity.

The heat conduction flux Φ between the two phases is defined as:

$$\Phi(T_\zeta) = \alpha_l \lambda Nu \frac{6}{d_l^2} (T_\zeta - T) \quad (\text{B.3})$$

where T_ζ is the droplet surface temperature and is equal to T_l as droplets are supposed to have uniform temperature.

The exact resolution of Eq. B.1 and Eq. B.2 is beyond the scope of this paper but a simple approximation of the gas temperature space shape within the depot can be obtained by replacing the ΔT term in Eq. B.1 by a simplified expression: if the temperature is supposed to follow a parabolic profile (Fig. 7) with a maximum value T at $r = 0$ and a temperature T_∞ at $r = d_k/2$, the Laplacien of T can be approximated by:

$$\Delta T = \frac{8n_{dim}(T_\infty - T)}{d_k^2} \quad (\text{B.4})$$

Assuming $Le = 1$ (i.e. $\frac{\lambda}{\rho C_p} = D$), Eq B.1 becomes:

$$\frac{\partial T}{\partial t} = \frac{8n_{dim}D(T_\infty - T)}{d_k^2} + \alpha_l D Nu \frac{6}{d_l^2} (T_l - T) + \frac{S}{\rho C_p} \quad (\text{B.5})$$

Then, introducing: $\tau_{cond} = \frac{d_l^2}{6\alpha_l D Nu}$ and $\tau_{diff} = \frac{d_k^2}{8n_{dim}D}$, Eq B.5 simplifies to:

$$\frac{\partial T}{\partial t} = \frac{1}{\tau_{diff}} (T_\infty - T) + \frac{1}{\tau_{cond}} (T_l - T) + \frac{S}{\rho C_p} \quad (\text{B.6})$$

Similarly, Eq B.2:

$$\frac{\partial T_l}{\partial t} = -A \frac{1}{\tau_{cond}} (T_l - T) \quad (\text{B.7})$$

where $A = \frac{\rho C_p}{\alpha l \rho_l C_{pl}}$

These equations are valid for the energy deposition (Phase 1 in Fig. 8) and the heating phase of the droplets (Phase 2 in Fig. 8), before they reach T_{cc} .

- Phase 1: energy deposition ($0 < t \leq t_d$):

$$S = \dot{e}_{dep}(x, t) \quad (\text{B.8})$$

Supposing in this phase that the liquid temperature is constant, equal to $T_{l,0}$, Eq B.6 writes:

$$\frac{\partial T}{\partial t} + \frac{1}{\tau} T = \frac{T_\infty}{\tau_{diff}} + \frac{T_{l,0}}{\tau_{cond}} + \frac{\dot{e}_{dep}(x, t)}{\rho C_p} \quad (\text{B.9})$$

where τ is defined as:

$$\frac{1}{\tau} = \frac{1}{\tau_{diff}} + \frac{1}{\tau_{cond}} \quad (\text{B.10})$$

The solution of Eq B.9 is:

$$T(t) = \left[T_\infty + \int_0^t \left(\frac{T_\infty}{\tau_{diff}} + \frac{T_{l,0}}{\tau_{cond}} + \frac{\dot{e}_{dep}(0, t')}{\rho C_p} \right) e^{\frac{t'}{\tau}} dt' \right] e^{-\frac{t}{\tau}} \quad (\text{B.11})$$

A quantitative analysis of the magnitude of the different terms shows that $\dot{e}_{dep}(0, t')$ is several orders greater than the other two terms which can be neglected. Consequently, at the end of the sparking time (i.e. at $t = t_d$):

$$T(t_d) = T_d = T_\infty + \frac{e_{dep}}{\rho C_p} \quad (\text{B.12})$$

where $e_{dep} = \int \dot{e}_{dep} dt$.

- Phase 2: droplet pre-heating ($t_d < t \leq t_{cc}$):

The second phase lasts from the end of the deposition at t_d , to the time t_{cc} when the temperature of the droplets reaches the saturation value T_{cc} (Fig. 8). In this phase, the energy source from spark is null ($S = 0$)

and the one from combustion is still negligible. Hence the temperature evolution of the gas phase is:

$$T(t^*) = \left[T_d + \int_0^{t^*} \left(\frac{T_\infty}{\tau_{diff}} + \frac{T_{l,0}}{\tau_{cond}} \right) e^{\frac{t'}{\tau}} dt' \right] e^{-\frac{t^*}{\tau}} \quad (\text{B.13})$$

where $t^* = t - t_d$

Then:

$$\begin{aligned} T(t_{cc}) &= \left[T_d + \int_0^{t_{cc}-t_d} \left(\frac{T_\infty}{\tau_{diff}} + \frac{T_{l,0}}{\tau_{cond}} \right) e^{\frac{t'}{\tau}} dt' \right] e^{-\frac{t_{cc}-t_d}{\tau}} \\ &= T^* + (T_d - T^*) e^{-\frac{t_{cc}-t_d}{\tau}} \end{aligned} \quad (\text{B.14})$$

where $T^* = \tau \left[\frac{T_\infty}{\tau_{diff}} + \frac{T_{l,0}}{\tau_{cond}} \right]$

Now that $T(t_{cc})$ is a function of t_{cc} , this last time has to be determined. Solving Eq. B.7 for $t_d \leq t \leq t_{cc}$, we obtain:

$$T_l(t^*) = \left[T_{l,0} + \int_0^{t^*} \frac{A}{\tau_{cond}} T(t') e^{\frac{A}{\tau_{cond}} t'} dt' \right] e^{-\frac{A}{\tau_{cond}} t^*} \quad (\text{B.15})$$

which leads to:

$$T_{cc} = T_l(t_{cc}) = \left[T_{l,0} + \int_0^{t_{cc}-t_d} \frac{A}{\tau_{cond}} T(t') e^{\frac{A}{\tau_{cond}} t'} dt' \right] e^{-\frac{A}{\tau_{cond}} (t_{cc}-t_d)} \quad (\text{B.16})$$

We suppose in this phase that the gas temperature varies slowly, and in order to integrate Eq. B.16, use $T(t) \approx T_d$. Hence:

$$T_{cc} = \left[T_{l,0} + T_d \left(e^{\frac{A}{\tau_{cond}} (t_{cc}-t_d)} - 1 \right) \right] e^{-\frac{A}{\tau_{cond}} (t_{cc}-t_d)} \quad (\text{B.17})$$

After some rearrangements, one obtains:

$$t_{cc} - t_d = -\frac{\tau_{cond}}{A} \text{Ln} \left(\frac{T_{cc} - T_d}{T_{l,0} - T_d} \right) \quad (\text{B.18})$$

As $T_{cc} - T_{l,0} \ll T_d - T_{l,0}$, a 1st order Taylor expansion gives:

$$t_{cc} - t_d = \frac{\tau_{cond}}{A} \frac{T_{cc} - T_{l,0}}{T_d - T_{l,0}} \quad (\text{B.19})$$

Including expressions in Eqs. B.12 - B.14 and B.19 in the criterion definition Eq. 3; and supposing that $T_{l,0}$ and T_∞ are close:

$$T(t_{cc}) \geq T_{ign} \iff T_\infty + \frac{e_{dep}}{\rho C_p} \exp\left(-\frac{\tau_{cond}}{A\tau} \frac{T_{cc} - T_{l,0}}{T_d - T_{l,0}}\right) \geq T_{ign} \quad (\text{B.20})$$

Which leads after another Taylor expansion on the exponential term and some rearrangements to:

$$e_{dep} \geq \rho C_p (T_{ign} - T_\infty) + \rho C_p \frac{\tau_{cond}}{A\tau} (T_{cc} - T_{l,0}) \quad (\text{B.21})$$

Finally, we have:

$$e_{dep} \geq \rho C_p (T_{ign} - T_\infty) + \left(\alpha_l + \frac{4n_{dim}}{3Nu} \frac{d_l^2}{d_k^2}\right) \rho_l C_{p,l} (T_{cc} - T_{l,0}) \quad (\text{B.22})$$

References

- [1] E. Mastorakos, *Progress in Energy and Combustion Science* 35 (2009) 57–97.
- [2] S. F. Ahmed, R. Balachandran, T. Marchione, E. Mastorakos, *Combust. Flame* 151 (2007) 366–385.
- [3] T. Marchione, S. F. Ahmed, E. Mastorakos, *Combustion and Flame* 156 (2008) 166–180.
- [4] R. Lecourt, Ignition and Extinction results at ambient conditions, Technical Report, Timecop Report No. 2.2.1a, 2008.
- [5] A. Neophytou, E. Mastorakos, R. Cant, *Combustion and Flame* 157 (2010) 1071–1086.
- [6] P. Boudier, S. Henriot, T. Poinsot, T. Baritaud, in: T. C. Institute (Ed.), *Twenty-Fourth Symposium (International) on Combustion*, pp. 503–510.
- [7] T. Kravchik, E. Sher, *Combust. Flame* 99 (1994) 635–643.
- [8] D. R. Ballal, A. H. Lefebvre, *Proc. R. Soc. Lond. A* 357 (1977) 163–181.
- [9] V. Quintilla, M. Cazalens, R. Lecourt, G. Lavergne, in: *15th International Symposium of Air Breathing Engines*.
- [10] N. Ouarti, Modélisation de l’allumage d’un brouillard de carburant dans un foyer de turbomachine, Ph.D. thesis, Université de Toulouse, 2004.
- [11] N. García-Rosa, Phénomènes d’allumage d’un foyer de turbomachine en conditions de haute altitude, Ph.D. thesis, Université de Toulouse, 2008.
- [12] D. R. Ballal, A. H. Lefebvre, *Proc. R. Soc. Lond. A* 364 (1978) 277–294.
- [13] D. R. Ballal, A. H. Lefebvre, in: T. C. Institute (Ed.), *Eighteenth Symposium (International) on Combustion*, pp. 1737–1747.
- [14] M. Boileau, G. Staffelbach, B. Cuenot, T. Poinsot, C. Bérat, *Combust. Flame* 154 (2008) 2–22.

- [15] S. Roux, G. Lartigue, T. Poinsot, U. Meier, C. Bérat, *Combust. Flame* 141 (2005) 40–54.
- [16] L. Selle, *Simulation aux grandes échelles des interactions flamme-acoustique dans un écoulement vrillé*, Phd thesis, INP Toulouse, 2004.
- [17] H. Forkel, J. Janicka, *Flow, Turb. and Combustion* 65 (2000) 163–175.
- [18] H. Pitsch, *Ann. Rev. Fluid Mech.* 38 (2006) 453–482.
- [19] V. K. Chakravarthy, S. Menon, *Flow, Turb. and Combustion* 65 (2000) 133–161.
- [20] G. Lacaze, E. Richardson, T. J. Poinsot, *Combust. Flame* 156 (2009) 1993–2009.
- [21] R. Lecourt, *Injection system two-phase flow characterization (LDA-PDA)*, Technical Report, Timecop Report No. 2.2.1c, 2009.
- [22] F. Ducros, F. Nicoud, T. Poinsot, in: *ICFD*, Baines M. J., 1998, pp. 293–300.
- [23] T. Poinsot, S. Lele, *J. Comput. Phys.* 101 (1992) 104–129.
- [24] J. Senoner, M. Sanjosé, T. Lederlin, F. Jaegle, M. García, E. Riber, B. Cuenot, L. Gicquel, H. Pitsch, T. Poinsot., *C. R. Acad. Sci. Mécanique* 337 (2009) 528–538.
- [25] T. M. Sloane, *Combust. Sci. Tech.* 73 (1990) 351–365.
- [26] M. Champion, B. Deshaies, G. G. Joulin, *Combust. Flame* 74 (1988) 161–170.
- [27] V. Subramanian, P. Domingo, L. Vervisch, *Combustion and Flame* 157 (2010) 579–601.
- [28] R. Maly, M. Vogel, in: *17th Symp. (Int.) on Combustion*, The Combustion Institute, Pittsburgh, 1978, pp. 821–831.
- [29] M. Kono, K. Hatori, K. Inuma, in: *20th Symp. (Int.) on Combustion*, The Combustion Institute, Pittsburgh, 1984, pp. 133–140.

- [30] M. Thielle, S. Selle, U. Riedel, J. Warnatz, U. Maas, in: T. C. Institute (Ed.), Twenty-Eighth Symposium (International) on Combustion, pp. 1177–1185.
- [31] R. Teets, J. Sell, SAE transactions 97 (1988) 371–383.
- [32] T. Phuoc, F. White, Proc. Combust. Inst. 29 (2002) 1621 – 1628.
- [33] B. Franzelli, E. Riber, M. Sanjosé, T. Poinso, Combust. Flame 157 (2010) 1364–1373.
- [34] C. Law, Combustion physics, Cambridge University Press, 2006.
- [35] D. B. Spalding, in: 4th Symp. (Int.) on Combustion, The Combustion Institute, Pittsburgh, 1953, pp. 847–864.
- [36] W. M. Huang, S. R. Vosen, R. Greif, in: 21st Symp. (Int.) on Combustion, The Combustion Institute, Pittsburgh, 1986, pp. 1853–1860.
- [37] S. R. Vosen, R. Greif, C. K. Westbrook, in: 20th Symp. (Int.) on Combustion, The Combustion Institute, Pittsburgh, 1984, pp. 76–83.
- [38] F. Dabireau, B. Cuenot, O. Vermorel, T. Poinso, Combust. Flame 135 (2003) 123–133.
- [39] A. Delataillade, F. Dabireau, B. Cuenot, T. Poinso, Proc. Combust. Inst. 29 (2002) 775–780.
- [40] A. Neophytou, Spark Ignition and Flame Propagation in Sprays, Ph.D. thesis, University of Cambridge, 2010.
- [41] R. G. Abdel-Gayed, D. Bradley, M. N. Hamid, M. Lawes, Proc. Combust. Inst. 20 (1984) 505–512.
- [42] O. Gulder, in: 23rd Symp. (Int.) on Comb., The Combustion Institute, Pittsburgh, Orleans, 1990, pp. 743–835.